Crystal Chemistry and Microwave Dielectric Properties of Ba₃MNb₂₋ₓSbₓO₉ (M = Mg, Ni, Zn)

Michael W. Lufaso,*,† Elizabeth Hopkins,† Steven M. Bell,‡ and Anna Llobet§

National Institute of Standards and Technology, Gaithersburg, Maryland, TCI Ceramics, Inc.,
Hagerstown, Maryland, and Los Alamos Neutron Science Center, Los Alamos National Laboratory,
Los Alamos, New Mexico

The effect of Sb^{5+} substitution on the crystal chemistry and dielectric properties of $Ba_3MNb_{2-x}Sb_xO_9$ (M = Mg, Zn, Ni) was investigated using a combination of X-ray and neutron powder diffraction, and dielectric property measurements at microwave frequencies. Rietveld refinements were carried out to characterize the crystal structures of $Ba_3ZnSb_2O_9$ and $Ba_3MgSb_2O_9$, which have a $6H-BaTiO_3$-type structure. Analyses of X-ray diffraction data of intermediate compositions evolve from a 2:1 ordered perovskite solid solution, to a two-phase ordered perovskite and 6H region, and also a 6H solid-solution for increasing Sb-content. Analysis of the bond distances indicates that the significant strain present in the 2:1 ordered perovskites is relieved in the 6H structure. Differences in the bonding preferences between the Nb^{5+} (d^0) and Sb^{5+} (d^{10}), combined with small changes in the ionic radii, influence the observed crystal chemistry. The magnitude and temperature dependence of the dielectric constant were lowest for compounds in the perovskite solid solution range with intermediate Sb^{5+} contents. $Ba_3MgNb_{1.75}Sb_{0.25}O_9$ ($\epsilon > 25$, $\tau_f \approx 6$ ppm K^{-1}, and $Qf > 96\,000$ GHz) and $Ba_3ZnNb_{1.625}Sb_{0.375}O_9$ ($\epsilon > 33$, $\tau_f \approx -3$ ppm K^{-1}, and $Qf > 44\,900$ GHz) display useful dielectric properties, rendering these materials suitable as lower-cost and lower-processing-temperature alternatives to perovskite tantalate ceramics.

Introduction

Inorganic ceramic oxides are used for microwave dielectric applications including filters, oscillators, and dielectric resonators in mobile and satellite telecommunications. Next-generation base stations may utilize ceramic oxide materials because of their low cost and high efficiency. In microwave dielectric resonator applications there are three physical properties that require optimization to meet the strict requirements of device applications.[1,2] One important physical property is the dielectric constant (ϵ). In many applications a larger dielectric constant is preferred because it allows miniaturization, all other factors being equal.[3] A second property is the temperature coefficient of the resonant frequency (τ_f) [τ_f is related to the temperature dependence of the dielectric constant (τ_ϵ) and the linear thermal expansion coefficient (α_1) by $\tau_f = -(\alpha_1 + \tau_\epsilon/2)$], which ideally has a near-zero value in units of ppm K^{-1}. Compositional tuning of τ_f through zero ppm K^{-1} in many perovskite materials can be accomplished by formation of a solid solution with appropriate cation substitution.[4] Dielectric loss, tan δ, is the third physical property requiring optimization and at microwave frequencies is often expressed using the quality factor,

$Q = (\tan \delta)^{-1}$. The quality factor multiplied by the resonant frequency, Qf, is approximately a constant for similarly sized samples and allows comparison of dielectric loss values between samples measured at different frequencies. A low dielectric loss (i.e., larger Qf) value is more desirable for device applications.

The perovskite structure type, ABO_3, and the ordering of the octahedrally coordinated M-site cations has been extensively studied.[5] When 2:1-type ordering[6] of the B-site cations occurs for $AM_{1/3}M'_{2/3}O_3$, the formula may be rewritten as $A_3MM'_2O_9$. The 2:1 ordered perovskites, $Ba_3MgTa_2O_9$ and $Ba_3ZnTa_2O_9$, exhibit exceptionally high Qf values which make them suitable for telecommunication applications where frequency selectivity is vital.[7,8] Significant efforts have been made to synthesize additional materials with comparable physical properties and reduced raw material and processing costs. Solid solutions on both the A and M site have been investigated to observe the effect on dielectric properties. One prospective system is based on the substitution of Nb^{5+} for Ta^{5+} in order to reduce materials cost and processing temperatures.[9] Complete substitution results in a higher dielectric constant; however, the τ_f values are more positive and the Qf values are lower. Solid solutions of two compounds with opposite signs of τ_f have been useful in

---

* To whom correspondence should be addressed at current affiliation: Department of Chemistry and Biochemistry, Columbia, SC. E-mail: lufaso@mail.chem.sc.edu.
  † National Institute of Standards and Technology.
  ‡ TCI Ceramics, Inc.
  § Los Alamos Neutron Science Center.

(1) Cava, R. J. *J. Mater. Chem.* **2001,** *11,* 54−62.
(2) Vanderah, T. A. *Science* **2002,** *298,* 1182−1184.
(3) Wersing, W. *Curr. Opin. Solid State Mater.* **1996,** *1,* 715−731.
(4) Vanderah, T. A.; Miller, V. L.; Levin, I.; Bell, S. M.; Negas, T. *J. Solid State Chem.* **2004,** *177,* 2023−2038.
(5) Anderson, M. T.; Greenwood, K. B.; Taylor, G. A.; Poeppelmeier, K. R. *Prog. Solid State Chem.* **1993,** *22,* 197−233.
(6) Lufaso, M. W. *Chem. Mater.* **2004,** *16,* 2148−2156.
(7) Nomura, S.; Toyama, K.; Kaneta, K. *Jpn. J. Appl. Phys. 2* **1982,** *21,* L624−L626.
(8) Kawashima, S.; Nishida, M.; Ueda, I.; Ouchi, H. *J. Am. Ceram. Soc.* **1983,** *66,* 421−423.
(9) Hughes, H.; Iddles, D. M.; Reaney, I. M. *Appl. Phys. Lett.* **2001,** *79,* 2952−2954.

producing temperature-compensated materials.[10] For example, tunability of τ_f has been demonstrated in the $Ba_3Co_{1-x}Zn_xNb_2O_9$ perovskite solid solution.[11-13]

Bonding preferences and the second-order Jahn−Teller distortion of d^0 Nb^{5+} and Ta^{5+} are important in stabilizing the out-of-center distortion of the octahedra that occurs in the 2:1 ordered perovskites. Only one compound with M^{5+} having a partially filled d-shell, $Sr_3CaRu_2O_9$, has been reported[14,15] to crystallize as a 2:1 ordered perovskite. Isostructural perovskite derivatives often form with complete substitution of Sb^{5+} for Nb^{5+} and Ta^{5+} because of the similar ionic radii and preferences for octahedral coordination. For example, Ba_2YSbO_6 and Ba_2YTaO_6 (space group $Fm\bar{3}m$),[16,17] Ca_2MnSbO_6 and Ca_2MnNbO_6 (space group $Pnma$),[18] Sr_2MnSbO_6 and Sr_2MnNbO_6 (space group $I4/mcm$),[18] and Ca_2FeSbO_6 and Ca_2FeNbO_6 (space group $P2_1/n$)[19,20] all crystallize as perovskite variants. $Ba_3MNb_2O_9$ (M = Mg, Ni, Zn) compounds crystallize as 2:1 ordered perovskites.[6] In contrast, $Ba_3MSb_2O_9$ (M = Mg, Ni, Zn) phases crystallize in space group $P6_3/mmc$ with a 6H−BaTiO₃-type crystal structure containing face-sharing [SbO₆] octahedral, with the M^{2+} ions occupying vertex sharing octahedra.[21] In this study, we report on the partial substitution of Sb^{5+} for Nb^{5+} in $Ba_3MNb_{2-x}Sb_xO_9$ (M = Mg, Ni, Zn), and the influence this has on the dielectric properties and crystal chemistry of the system. Crystal structures of $Ba_3MSb_2O_9$ (M = Mg, Zn) refined from neutron powder diffraction data are also reported.

Experimental Techniques

Polycrystalline samples of $Ba_3MgNb_{2-x}Sb_xO_9$ (x = 0.125, 0.25, 0.5, 1.0, 1.875), $Ba_3NiNb_{2-x}Sb_xO_9$ (x = 0.1, 0.25, 0.5, 0.75, 1.0, 1.875), and $Ba_3ZnNb_{2-x}Sb_xO_9$ (x = 0.125, 0.25, 0.375, 0.5, 0.75, 1.0, 1.875) were prepared by conventional solid-state synthesis using high purity starting materials: $BaCO_3$ (Alfa Aesar, 99.95%), Nb_2O_5 (Alfa Aesar, 99.9985%), Sb_2O_3 (Alfa Aesar, 99.999%), NiO (Alfa Aesar, 99.998%), $MgCO_3 \cdot xH_2O$ (99.996%, Alfa Aesar, preanalyzed by TGA), and ZnO (Alfa Aesar, 99.99%). Appropriate molar ratios of the oxides and carbonates were weighed and mixed with an agate mortar and pestle. Uniaxially pressed pellets were placed on a sacrificial powder of the same composition on top of platinum foil on an alumina plate. Samples were calcined overnight at 900 °C and subsequent heating performed with intermediate grindings until the samples reached equilibrium, which was assumed to occur when no further changes were evident in the relative intensities of the diffraction peaks in laboratory X-ray diffraction measurements. Synthesis temperatures were 1250 °C (M = Zn), 1350−1500 °C (M = Ni), and 1450−1550 °C (M = Mg). X-ray data were collected using a Philips diffractometer equipped with incident Soller slits, theta compensating divergence slit, graphite monochromator, and scintillation detector. Lattice parameters were corrected for curvature by applying an external parabolic calibration correction in the MDI Jade software using SRM LaB_6 as the reference pattern.

Preparation of sufficiently dense (>90%) pellets for dielectric measurements was not accomplished by increasing sintering temperatures. Instead, polycrystalline samples were milled with yttria stabilized zirconia grinding media for 15 min in ethanol. The powders were dried, uniaxially pressed, and then isostatically pressed into cylindrical disks under a pressure of 175 MPa. Pellets were preheated to 300 °C to remove any residual solvent and covered with an inverted crucible to minimize cation volatility at the elevated sintering temperatures. Sintering was performed in air for between 4 and 8 h at temperatures of 1450 °C for M = Zn, 1515 °C for M = Ni, and 1575 °C for M = Mg. Typical observed densities of the sintered pellets were greater than 95% for perovskite solid solutions, but were not determined for the two-phase region because of the imprecise value of the theoretical density. The theoretical densities were calculated from the lattice parameters derived from X-ray diffraction measurements.

Time-of-flight neutron powder diffraction data were collected on the high-intensity powder diffractometer (HIPD) at Los Alamos Neutron Science Center. Detector banks are located at ±153°, ±90°, ±40°, and ±14°. Samples were contained in a vanadium sample cylinder. Data were collected for ca. 2 h at ambient temperature. The General Structure Analysis System (GSAS) and the EXPGUI interface was used for Rietveld structural refinements.[22,23] Default neutron scattering amplitudes were used in the refinements. Statistical uncertainties quoted in all of the results represent one standard deviation.

Dielectric properties were measured using a cylindrical resonant cavity with an HP 8720D Vector Network Analyzer. Samples were sintered cylindrical pellets machined to have a diameter/height ratio of approximately 2.5:1; they ranged from 9.9 to 12.6 mm in diameter and from 4.1 to 6.9 mm in height. The dielectric constants of most compositions were obtained with machined samples of a diameter of 6.1 mm and height of 4.32 mm and measurement by the Courtney method.[24] Also, the dielectric constants were estimated from sample size and frequency of the $TE_{01\delta}$ resonance mode. Uncertainty of the dielectric constant is estimated to be less than 1%. Unloaded Q values were measured using the transmission method with an estimated uncertainty in Qf of less than 5%. The Qf measurements were made at ambient temperature and τ_f measurements for each compound were obtained at 25 and 60 °C in gold-plated aluminum cavities in a Tenney environmental chamber. The reproducibility in τ_f is estimated to be ±1 ppm K^{-1}.

Results and Discussion

Crystal Structure and Phase Analysis. Indexing of X-ray powder diffraction data of $Ba_3MNb_2O_9$ (M = Mg, Ni, Zn) was consistent with a 2:1 cation ordered perovskite with space group $P\bar{3}m1$. For $Ba_3MSb_2O_9$ (M = Mg, Ni, Zn) the

(10) Wise, P. L.; Reaney, I. M.; Lee, W. E.; Iddles, D. M.; Cannell, D. S.; Price, T. J. *J. Mater. Res.* **2002**, *17*, 2033−2040.

(11) Scott, R. I.; Thomas, M.; Hampson, C. *J. Eur. Ceram. Soc.* **2003**, *23*, 2467−2471.

(12) Endo, K.; Fujimoto, K.; Murakawa, K. *J. Am. Ceram. Soc.* **1987**, *70*, C215−C218.

(13) Yue, Z. X.; Zhao, F.; Zhang, Y. C.; Gui, Z. L.; Li, L. T. *Mater. Lett.* **2004**, *58*, 1830−1834.

(14) Rijssenbeek, J. T.; Malo, S.; Caignaert, V.; Poeppelmeier, K. R. *J. Am. Chem. Soc.* **2002**, *124*, 2090−2091.

(15) Rijssenbeek, J. T.; Saito, T.; Malo, S.; Masaki, A. T.; Takano, M.; Poeppelmeier, K. R. *J. Am. Chem. Soc.* **2005**, *127*, 675−681.

(16) Alonso, J. A.; Cascales, C.; Casado, P. G.; Rasines, I. *J. Solid State Chem.* **1997**, *128*, 247−250.

(17) Fujii, T.; Takahashi, J.; Shimada, S.; Kageyama, K. *J. Electroceram.* **1999**, *3*, 387−397.

(18) Lufaso, M. W.; Woodward, P. M.; Goldberger, J. *J. Solid State Chem.* **2004**, *177*, 1651−1659.

(19) Lee, S. O.; Cho, T. Y.; Byeon, S. H. *Bull. Korean Chem. Soc.* **1997**, *18*, 91−97.

(20) Chakhmouradian, A. R.; Mitchell, R. H. *J. Solid State Chem.* **1998**, *138*, 272−277.

(21) Treiber, U.; Kemmlersack, S. *Z. Anorg. Allg. Chem.* **1982**, *487*, 161−177.

(22) Larson, A. C.; von Dreele, R. B. *General Structure Analysis System (GSAS)*; Los Alamos National Laboratories: Los Alamos, NM, 1990.

(23) Toby, B. H. *J. Appl. Crystallogr.* **2001**, *34*, 210−213.

(24) Courtney, W. E. *IEEE Trans. Microwave Theory Technol.* **1970**, *18*, 476−485.
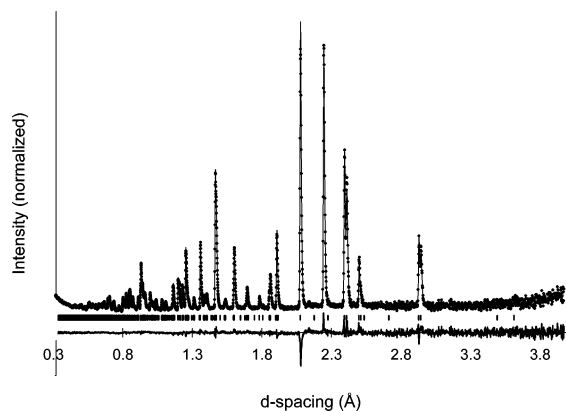
Figure 1. Ambient temperature powder neutron diffraction data for $Ba_3ZnSb_2O_9$. Circles are collected data, solid lines are fitted. Differences between observed and calculated intensities are shown below. Vertical marks indicate calculated peak positions. Normalized data are shown for the detector at +153°.

Table 1. Refined Structural Parameters and Reliability Factors for $Ba_3MSb_2O_9$ (M = Mg, Zn)[a]

exp	$Ba_3MgSb_2O_9$	$Ba_3ZnSb_2O_9$
a (Å)	5.8441(2)	5.8538(1)
c (Å)	14.4089(6)	14.4498(3)
Ba2 z	0.90892(23)	0.91015(12)
Sb^{5+} z	0.15072(20)	0.15179(9)
O1 x	0.48075(24)	0.48087(11)
O1 y	−0.0385(5)	−0.03825(23)
O2 x	0.16948(23)	0.16926(11)
O2 z	0.41614(12)	0.41566(6)
R_p (profile) (%)	0.71	1.56
R_{wp} (weighted profile) (%)	0.98	2.03
R^2F (Bragg) Bank 1 (%)	3.34	3.04
reduced χ^2 (%) (8 Banks)	1.05	2.73
Sb−O(1) (Å) (×3)	2.067(3)	2.062(1)
Sb−O(2) (Å) (×3)	1.918(2)	1.928(1)
M^{2+}−O(2) (Å) (×6)	2.098(2)	2.1049(9)
Sb−O(1)−Sb (deg)	87.58(14)	86.98(7)

[a] The fixed atomic fractional coordinate positions are Ba1[2b] (0, 0, $1/4$), Ba2[4f] ($1/3$, $2/3$, z), M^{2+}[2A] (0, 0, 0), M^{5+}[4f] ($1/3$, $2/3$, z), O1[6h] (x, y, $1/4$) and O2[12k] (x, 2x, z) in space group $P6_3/mmc$.

data were consistent with a 6H structure type with space group $P6_3/mmc$. Crystal structures of $Ba_3MNb_2O_9$ (M = Mg, Ni, Zn)[6] and $Ba_3NiSb_2O_9$[25] have been previously reported from refinements of neutron powder diffraction data. The structures of $Ba_3MgSb_2O_9$ and $Ba_3ZnSb_2O_9$ were refined using time-of-flight neutron powder diffraction data. Rietveld refinements were performed using the lattice parameters refined from X-ray powder diffraction data and the fractional coordinates corresponding to those of $Ba_3NiSb_2O_9$.[25] The neutron powder diffraction pattern and refined model for $Ba_3ZnSb_2O_9$ are presented in Figure 1. $Ba_3MgSb_2O_9$ and $Ba_3ZnSb_2O_9$ are both well described by the 6H structure type. Structural parameters, bond lengths, and refinement details are shown in Table 1. The crystal structure of $Ba_3MgSb_2O_9$ is presented in Figure 2 and is described as a 6-layer structure with mixed hexagonal and cubic stacking of $[BaO_3]$ layers, in contrast to the cubic stacking of perovskites. The face-sharing $[Sb_2O_9]$ groups are linked through a single $[M^{2+}O_6]$ octahedra. Face-sharing creates cation−cation (Sb^{5+}−Sb^{5+}) repulsion, which is evident in the Sb−O bond distances shown in Table 1.
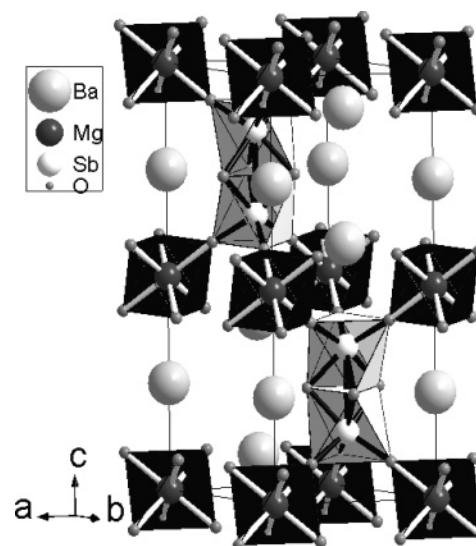
Figure 2. Crystal structure of $Ba_3MgSb_2O_9$. Atom types are shown in the inset and the unit cell is outlined. SbO_6 octahedra are lightly shaded and MgO_6 octahedra are darkly shaded.

Bonding differences between the Nb^{5+} (d^0) and Sb^{5+} (d^{10}) play a role in stabilizing the 6H− structure as an alternative to the perovskite structure. M^{5+}−O−M^{5+} bond angles are approximately 180° for $Ba_3MNb_2O_9$ (M = Mg, Ni, Zn) perovskites, whereas the M^{5+}−O−M^{5+} bond angle is approximately 90° for $Ba_3MSb_2O_9$ (M = Mg, Ni, Zn). The empty d-orbitals on Nb^{5+} and second-order Jahn−Teller distortion assist the out of center distortion and π bonding with the 2p orbitals on oxygen. Stronger covalent bonding of an anion is present if different orbitals are used in the formation of each cation−anion bond, and this effect is reduced if the cations have empty d-orbitals available for π bonding. Stabilization of d^{10} Sb^{5+} with face-sharing $[Sb_2O_9]$ units and Sb−O−Sb bond angles at approximately 90° optimizes σ bonding with two different O 2p orbitals. Because Sb^{5+} has a filled d shell, no π bonding is possible and the formation of 180° Sb^{5+}−O−Sb^{5+} bond linkages are inhibited compared to Nb^{5+}−O−Nb^{5+}. In addition, $Sr_3NiSb_2O_9$ has Sb^{5+} in a corner-sharing octahedron of the perovskite with an octahedral tilting distortion that decreases the M−O−M bond angles from 180°.[26] Although it is rare, it is noted that 180° Sb^{5+}−O−Sb^{5+} bonds are found in the perovskites $Ba_4LiSb_3O_{12}$ and $Ba_4NaSb_3O_{12}$.[27] Stabilization of face-sharing octahedra does not appear to occur solely because of differences in bonding preferences. Six coordinate Sb^{5+} adopts both face-sharing coordination environments with ≈90° Sb^{5+}−O−Sb^{5+} bond angles and also corner-sharing environments with ≈180° Sb^{5+}−O−Sb^{5+} bond angles. The stability of compounds containing Sb^{5+}−O−Sb^{5+} bonds has been qualitatively described in terms of relative ionic sizes, Madelung energy, polarizability of A-cation cores, and covalent contribution to M−O bonds.[28,29] The contribution from each of these factors subtly controls the crystal chemistry in the systems of this study.

(25) Jacobson, A. J.; Calvert, A. J. *J. Inorg. Nucl. Chem.* **1978**, *40*, 447−449.

(26) James, M.; Attfield, J. P.; Rodriguez-Carvajal, J. *J. Phys. Chem. Solids* **1995**, *56*, 1331−1337.

(27) Alonso, J. A.; Mzayek, E.; Rasines, I. *Mater. Res. Bull.* **1987**, *22*, 69−74.

Table 2. Chemical Formula, Tolerance Factors, Space Groups, M−O−M Bond Angles, and Structure Types for Select Compounds

	tolerance factor	space group	M−O−M(5+) bond angle	structure type
BaTiO$_3$	1.071	$P6_3/mmc$	84.97(1)	6H[40]
Ba$_3$NiSb$_2$O$_9$	1.057	$P6_3/mmc$	87.01(1)	6H[25]
Ba$_3$MgSb$_2$O$_9$	1.052	$P6_3/mmc$	87.58(14)	6H
Ba$_3$ZnSb$_2$O$_9$	1.048	$P6_3/mmc$	86.98(7)	6H
Ba$_3$NiNb$_2$O$_9$	1.043	$P\bar{3}m1$	175.91(13)	perovskite[6]
Ba$_3$MgNb$_2$O$_9$	1.038	$P\bar{3}m1$	175.23(9)	perovskite[6]
Ba$_3$ZnNb$_2$O$_9$	1.034	$P\bar{3}m1$	176.11(1)	perovskite[6]
Sr$_2$MnSbO$_6$	1.000	$I4/m$	166.3(1)	perovskite[18]
Sr$_3$NiSb$_2$O$_9$	0.996	$Pnnm$	168.6(1)	perovskite[26]
Ca$_2$MnSbO$_6$	0.964	$Pnma$	151.2(2), 151.9(1)	perovskite[18]

Table 3. Bond Valence Sum (vu) and Global Instability Index (GII) Values for Ba$_3$MM$'_2$O$_9$ (M = Mg, Ni, Zn; M$'$ = Nb, Sb)^a

	Ba$_3$MgNb$_2$O$_9$	Ba$_3$NiNb$_2$O$_9$	Ba$_3$ZnNb$_2$O$_9$
Ba1	2.41	2.48	2.38
Ba2	2.31	2.36	2.28
M^{2+}	1.96	1.84	1.98
M^{5+}	4.66	4.66	4.65
O1	2.00	2.05	2.01
O2	2.05	2.04	2.03
GII	0.211	0.239	0.204

	Ba$_3$MgSb$_2$O$_9$	Ba$_3$NiSb$_2$O$_9$	Ba$_3$ZnSb$_2$O$_9$
Ba1	2.06	2.12	2.05
Ba2	1.96	2.06	1.92
M^{2+}	2.01	1.92	2.03
M^{5+}	5.34	5.30	5.28
O1	2.10	2.12	2.10
O2	2.06	2.04	2.03
GII	0.139	0.132	0.119

^{a} Crystal structures were refined using neutron powder diffraction data.

Influence of the slight ionic radii[30] differences between octahedrally coordinated Sb^{5+} (0.74 Å) and Nb^{5+} (0.78 Å) was considered by calculating the AMO$_3$ perovskite tolerance factor, $t = (R_A + R_O)/\sqrt{2}(R_M + R_O)$, which describes the fit of the A-site cation within the corner-sharing network.[31] The ideal perovskite occurs near $t = 1$, and octahedral tilting distortions typically occur for $t < 1$. Table 2 shows tolerance factors, space groups, M−O−M bond angles, and structure type for selected compositions. As the tolerance factor increases, the perovskite structure type becomes less favored relative to the 6H type. The 6H structure type is able to accommodate the relatively large A-site ion by an expansion along the c-axis with minimal perturbation of the local octahedral coordination environment of the M-site ions, whereas increased bond strain occurs from compression of the A−O bonds and lengthening of the M−O bonds from ideal lengths occurs for $t > 1$ in perovskites. Bond valence sums (BVS), given in valence units (vu), of the ions from the refined crystal structures are shown in Table 3. The perovskites exhibit BVS for Ba that are significantly larger, whereas the BVS for Ba in the 6H-type crystal structures are smaller and closer to the formal oxidation state. The oversized Ba ions in the perovskites cause a stretching of the octahedral, which is evident in the smaller than ideal BVS of the M-site cations. The freedom for expansion along
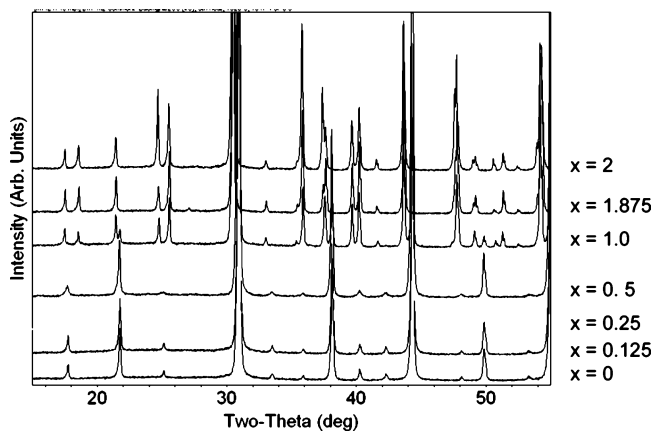
Figure 3. Portion of the X-ray powder diffraction pattern for Ba$_3$Mg-Nb$_{2-x}$Sb$_x$O$_9$ ($0 \leq x \leq 2$) demonstrating the progression from a perovskite ($0 < x \leq 0.5$), through a two-phase mixture ($x = 1$), to a 6H phase ($x \geq 1.875$).

the c-axis in the 6H structure is evident in the M-site cations having BVS nearer the formal values and a slight compression indicated for [SbO$_6$]. In both series of compounds, the BVS of O remains near the ideal formal value. The global instability index (GII)[32] is relatively large in the perovskites, and is near the value which has been described as the threshold of stability; i.e., values greater than 0.2 vu often lead to instability.[33] Partial substitution of the slightly smaller Sb^{5+} for Nb^{5+} increases tolerance factors and the GII because of the constraints of the corner-sharing connectivity in the perovskite. Crystallization in the 6H or perovskite systems is influenced by the additional bond strain present with increased M = Sb^{5+} substitution. Similarly, the bonding preference differences reinforce the 6H structure for the Sb^{5+} end member and perovskite structure for M = Nb^{5+}.

X-ray powder diffraction analysis was performed to establish the phases present. Figure 3 shows the X-ray diffraction pattern of Ba$_3$MNb$_{2-x}$Sb$_x$O$_9$ (M = Mg) for different compositions, which is representative of that observed in the analogous M = Ni, Zn compounds. Perovskite solid solution ranges are $0 < x < \approx 0.75$ for M = Mg and $0 < x < \approx 0.45$ for M = Ni, Zn in Ba$_3$MNb$_{2-x}$Sb$_x$O$_9$. Mixed perovskite and 6H-type phase regions are observed for $\approx 0.75 < x < \approx 1.5$ for M = Mg and $\approx 0.45 < x < \approx 1.5$ for M = Ni, Zn in Ba$_3$MNb$_{2-x}$Sb$_x$O$_9$. 6H-type solid solution ranges are observed for $\approx 1.5 < x < 2$ for M = Mg, Ni, and Zn in Ba$_3$MNb$_{2-x}$Sb$_x$O$_9$. Observation of a perovskite solid-solution, two phase region, and 6H-type ranges are consistent with the subtle factors controlling the transition from perovskite to 6H-type. Transition to a perovskite from a 6H− structure was reported in the high-pressure and high-temperature synthesis of Ba$_3$ZnSb$_2$O$_9$.[34] Stability difference between the two structure types is relatively small.

Cation ordering in perovskites results from differences in charge, ionic size, and bonding. Long-range cation order in the 2:1 ordered perovskites may be estimated by the c/a

(28) Goodenough, J. B.; Kafalas, J. A. *J. Solid State Chem.* **1973**, *6*, 493−501.
(29) Mizoguchi, H.; Woodward, P. M.; Byeon, S. H.; Parise, J. B. *J. Am. Chem. Soc.* **2004**, *126*, 3175−3184.
(30) Shannon, R. D. *Acta Crystallogr., Sect. A* **1976**, *32*, 751−767.
(31) Goldschmidt, V. M. *Naturwissenschaften* **1926**, *14*, 477.

(32) Salinas-Sanchez, A.; Garcia-Munoz, J. L.; Rodriguez-Carvajal, J.; Saez-Puche, R.; Martinez, J. L. *J. Solid State Chem.* **1992**, *100*, 201−211.
(33) Rao, G. H.; Barner, K.; Brown, I. D. *J. Phys.: Condens. Matter* **1998**, *10*, L757−L763.
(34) Battle, P. D.; Jones, C. W.; Lightfoot, P. *J. Solid State Chem.* **1990**, *85*, 144−150.
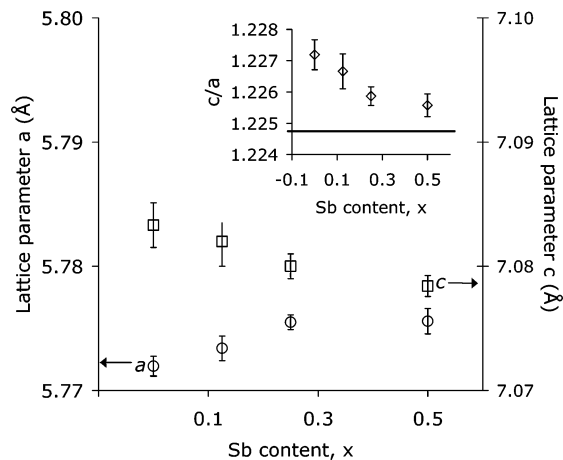
Figure 4. Lattice parameters are shown for $Ba_3MgNb_{2-x}Sb_xO_9$ in the perovskite solid-solution range. The c/a ratio is shown in the inset. Symbols: open squares for the c-axis and open circles for the a-axis.

lattice parameter ratio, which becomes larger than $\sqrt{(3/2)}$ with increased cation order. The c/a ratio has been found to directly correlate with the long-range order parameter.[35] A reduced c/a ratio is an indication that long-range cation order decreases with increased Sb content in the $Ba_3MgNb_{2-x}Sb_xO_9$ series shown in Figure 4. The tendency for Nb^{5+} to undergo a larger out of center distortion than Sb^{5+} may also play a role in the smaller c/a lattice parameter ratio; therefore, preferential site occupation of Sb^{5+} in the 6H phase and Nb^{5+} in the perovskite phase cannot be ruled out.

Dielectric Properties. Dielectric constants obtained from measurements at microwave frequencies are shown in Table 4. In the perovskite solid solution range, increased substitution of Sb corresponds to a smaller dielectric constant. The two-phase region flattens out, with minor changes in ϵ with composition. End member and 6H− solid solution range materials were not investigated in detail because of the smaller dielectric constant and difficulty in obtaining well-sintered materials for the measurement. Figure 5 shows τ_f as a function of x value in $Ba_3MNb_{2-x}Sb_xO_9$ (M = Mg, Ni, Zn). Increasing substitution of Sb in the perovskite solid solution range resulted in a less positive τ_f. Compositional tuning of τ_f through zero, forming a temperature-compensated material, is demonstrated in the perovskite solid solution range for $Ba_3MNb_{2-x}Sb_xO_9$ (M = Mg, Zn), whereas the negative τ_f of $Ba_3NiNb_{2-x}Sb_xO_9$ becomes increasingly negative in the perovskite solid solution range. A trendline is shown for $Ba_3ZnNb_{2-x}Sb_xO_9$, where a temperature-compensated material is expected to form in a compound with $x \approx 0.33$.

General trends observed with τ_f and ϵ are consistent with the observations in a wide variety of materials in that as the ϵ increases, the temperature dependence of the dielectric constant (τ_ϵ) tends to become more negative.[36] Tunability of τ_f in perovskites and related compounds has been attributed to two mechanisms: (1) dilution of the average ionic polarizability and (2) onset of an octahedral tilt transition above room temperature.[10,37,38] Tolerance factors

(35) Kim, I. T.; Oh, T. S.; Kim, Y. H. *J. Mater. Sci. Lett.* **1993**, *12*, 182−184.
(36) Harrop, P. J. *J. Mater. Sci.* **1969**, *4*, 370−374.

Table 4. Dielectric Properties of $Ba_3MNb_{2-x}Sb_xO_9$ (M = Mg, Ni, Zn)

	phase	ϵ_r	τ_f (ppm K^{-1})	Qf (f, GHz)
		x, M = Mg		
2	6H	21.5	−5.5	23 020 (5.1)
1.875	6H	15.0	2.8	84 100 (7.2)
1	6H,P	16.3	−4.1	33 410 (6.7)
0.5	P	14.7	4.8	81 310 (6.3)
0.25	P	25	6.4	96 290 (5.6)
0.125	P	28.5	14	101 300 (4.7)
0[b]	P	32	25	78 200
		x, M = Ni		
2	6H	14	−4.7	41 840 (7.8)
1.875	6H	14.8	−10	38 380 (6.8)
1	6H,P	20.4	−18	43 880 (6.3)
0.75	6H,P	18.7	−26.6	16 780 (6.0)
0.5	6H,P	20.2	−28.5	16 780 (5.7)
0.25	P	27	−20.6	27 370 (5.0)
0.1	P	26.5	−13.1	31 110 (5.0)
0[b]	P	31	−10	51 000
		x, M = Zn		
2	6H	13		1550 (7.7)
1.875	6H	12.5		2290 (7.6)
0.75	6H,P	30.9	−11.9	26 400 (5.5)
0.5	6H,P	30.9	−11.2	35 620 (5.3)
0.375	P	33.2	−2.8	44 940 (5.1)
0.25	P	35.8	6.2	35 090 (5.4)
0.125	P	35.7	13.9	56 980 (4.8)
0[b]	P	40.3	26	65 000

[a] The measurement frequency is given in parentheses. Phase abbreviations are 6H for 6H−$BaTiO_3$-type, P for 2:1 ordered perovskite, and 6H,P for mixed 6H−$BaTiO_3$-type and 2:1 ordered perovskite phase. [b] Average literature dielectric properties.[6]
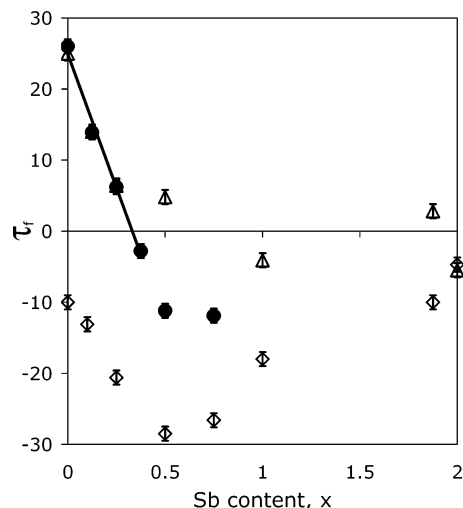
Figure 5. Temperature coefficient of the resonant frequency (τ_f) as a function of x value in $Ba_3MNb_{2-x}Sb_xO_9$ (M = Mg, Ni, Zn). Symbols: triangles, M = Mg; diamonds, M = Ni; and filled circles, M = Zn.

greater than unity in the compounds of this study rule out the possibility for an octahedral tilting transition; therefore, the primary mechanism of τ_f tunability is attributed to a reduction of the average ionic polarizability. The less positive τ_f with increased Sb content shown in Figure 5 is consistent with modification of τ_f via dilution of the dielectric constant as shown in Table 4.

Qf as a function of x value in $Ba_3MNb_{2-x}Sb_xO_9$ (M = Mg, Ni, Zn) is shown in Figure 6. A trend is found in which

(37) Reaney, I. M.; Wise, P.; Ubic, R.; Breeze, J.; Alford, N. M.; Iddles, D.; Cannell, D.; Price, T. *Philos. Magn. A* **2001**, *81*, 501−510.
(38) Wise, P. L.; Reaney, I. M.; Lee, W. E.; Price, T. J.; Iddles, D. M.; Cannell, D. S. *J. Eur. Ceram. Soc.* **2001**, *21*, 2629−2632.
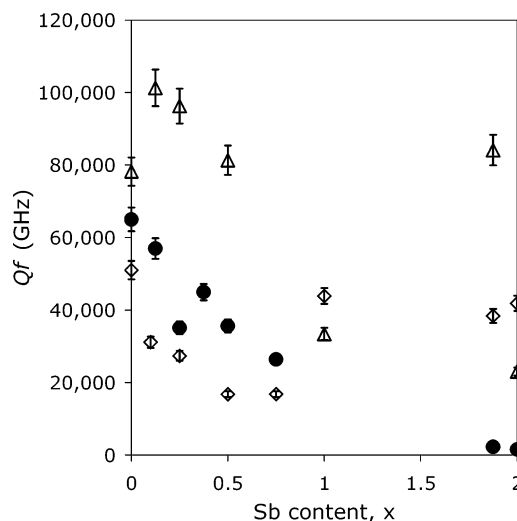
Figure 6. *Qf* as a function of *x* value in Ba$_3$MNb$_{2-x}$Sb$_x$O$_9$ (M = Mg, Ni, Zn). Symbols: triangles, M = Mg; diamonds, M = Ni; and filled circles, M = Zn.

Qf tends to decrease with increased Sb substitution. The compound with M = Ni has the smallest *Qf* values, M = Zn is intermediate, and M = Mg has the largest value. The M-site cation order has been attributed to play a role in determining *Qf*, with a higher degree of order displaying a larger *Qf*.[39] Smaller *c/a* lattice parameter ratios from X-ray diffraction data shown in Figure 3 indicate decreased cation order and the reduced *Qf* are consistent with previously observed trends in the dielectric properties of perovskites. Table 4 contains the ϵ_r, τ_f, and *Qf* value for compounds in this study measured at microwave frequencies. These *Qf* values are comparable with those of known perovskite materials, and allow the formation of a Ta-free temperature-compensated material.

Conclusions

The crystal chemistry and microwave dielectric properties of Ba$_3$MNb$_{2-x}$Sb$_x$O$_9$ (M = Mg, Zn, Ni) were investigated using X-ray powder diffraction and microwave dielectric property measurements. Time-of-flight neutron powder diffraction data were collected and Rietveld refinements were performed for Ba$_3$ZnSb$_2$O$_9$ and Ba$_3$MgSb$_2$O$_9$ to obtain accurate crystal structures and bond lengths. X-ray diffraction was used to obtain the composition of the phases as a function of *x* in Ba$_3$MNb$_{2-x}$Sb$_x$O$_9$ (M = Mg, Ni, Zn). Differences in ionic size and bonding preferences of Nb^{5+}

(d^0) and Sb^{5+} (d^{10}) play important roles in controlling the observed crystal chemistry. Ionic size differences between Sb^{5+} and Nb^{5+} appear to drive the formation of a perovskite solid solution, a two-phase mixture, and a 6H solid solution with increasing Sb^{5+} substitution. With larger *x*-values, the tolerance factors decrease and bond strain increases in the perovskite solid solution region. A bond valence sum analysis illustrates that the large amount of bond strain present in the 2:1 perovskite compounds is relieved in the 6H structure type. The 6H structure type allows lattice expansion, particularly along the *c*-axis, to accommodate the relatively large Ba^{2+} and significantly reduce bond strain. Simultaneously, the bonding preferences for Sb^{5+} are optimized for σ bonding with 2 different O 2p orbitals in the face-sharing octahedral coordination.

Compounds in the Ba$_3$MNb$_{2-x}$Sb$_x$O$_9$ (M = Mg, Ni, Zn) series enable tuning of the crystal chemistry, ϵ, τ_f, and *Qf*. Substitution of the appropriate level of Sb^{5+} into Ba$_3$MNb$_{2-x}$Sb$_x$O$_9$ (M = Mg, Ni, Zn) enables formation of perovskite solid solutions with tunable τ_f. Temperature-compensated compositions occur for the M = Zn, Mg series. Both Ba$_3$MgNb$_{1.75}$Sb$_{0.25}$O$_9$ ($\epsilon > 25$, $\tau_f \approx 6$ ppm K^{-1}, and *Qf* > 96 000 GHz) and Ba$_3$ZnNb$_{1.625}$Sb$_{0.375}$O$_9$ ($\epsilon > 33$, $\tau_f \approx -3$ ppm K^{-1}, and *Qf* > 44 900 GHz) display useful dielectric properties with lower processing temperatures and potentially lower production costs compared to tantalum-containing perovskite materials. Clearly, further processing studies would be beneficial to obtain optimal conditions, i.e., sintering duration, temperature, heating and cooling rates, and atmosphere for high-density ceramics with improved dielectric properties (i.e., larger ϵ and *Qf*). The phases Ba$_3$MM′$_2$O$_9$ (M = Co, Mg, Ni, Zn; M′ = Nb, Sb, Ta) provide a substantial opportunity to investigate subtle changes in crystal chemistry and properties, and may also provide materials with interesting and functional physical properties.

Supporting Information Available: Crystallographic information files (CIF) for Ba$_3$ZnSb$_2$O$_9$ and Ba$_3$MgSb$_2$O$_9$. Table containing additional crystallographic refinement details and thermal parameters (pdf). This material is available free of charge via the Internet at http://pubs.acs.org.

CM050631Y

(39) Davies, P. K.; Tong, J. Z.; Negas, T. *J. Am. Ceram. Soc.* **1997**, *80*, 1727−1740.
(40) Kwei, G. H.; Lawson, A. C.; Billinge, S. J. L.; Cheong, S. W. *J. Phys. Chem.* **1993**, *97*, 2368−2377.